Academic Journal of Science and Technology
ISSN: 2771-3032 | Vol. 10, No. 3, 2024

Combined Control Strategy of Wind Storage Based on Power Electronic Transformer

Rui Zhang*, Yan Xia, Huizhu Li, Yang Chen

Sichuan University of Science & Engineering, School of Automation and Information Engineering, Yibin, 643000, China
* Corresponding author: Zhang Rui (321081104118@stu.suse.edu.cn)

Abstract: Because of the inherent randomness and instability of the wind power generation system, the energy storage device and power electronic transformer are introduced into the wind power generation system to restrain the fluctuation of DC bus voltage and power junction, and improve the stability of the wind power generation system. This paper first introduces the basic characteristics of wind turbines and the basic idea of maximum wind energy capture and puts forward the control strategy of wind turbine side converter and grid side converter. Then the topological structure, mathematical model, and working principle of the power electronic transformer are described, and the control strategy of the power electronic transformer is proposed. Finally, the power electronic transformer is applied to the grid-connected wind storage system, and the grid-connected wind storage system model is built in MATLAB/Simulink platform, and the grid-connected control strategy under wind power fluctuation is simulated and verified. The simulation results show that the topology structure of the grid-connected wind storage system and the effectiveness of the grid-connected control strategy are proposed.

Keywords: Wind power generation system, Energy storage equipment, Power electronic transformer, Decoupling control.

1. Introduction

Due to the instability and uncertainty of wind energy, a series of problems will occur when large-scale wind power generation is integrated into the power grid. To improve the utilization rate of wind energy and increase the acceptable penetration rate of wind power in the power grid, it is necessary to study methods that can effectively calm wind power fluctuations. The methods for smoothing wind power can be roughly divided into two categories. The first is to rely only on the smooth control of the fan itself, that is, to rely on variable speed control[1] or variable pitch Angle control[2] to smooth the active power output of the fan. Although it can smooth the active power output of the fan, it also reduces the efficiency of wind energy capture to a certain extent. The second type relies on the smooth control of the energy storage system[3-5], which is a widely used calming method because it can ensure a high efficiency of wind energy capture and smooth the active power output of the fan.

The energy storage system includes a power converter and an energy storage unit. Through the effective control of the power converter, the energy storage and release of the entire system can be realized[6]. However, both the power converter and the grid-connected converter cannot be separated from the support of power electronics technology. The topology of a power electronic transformer includes AC/DC transformation of the rectifier stage, DC/AC/AC/ AC/DC transformation of the isolation stage, and DC/AC transformation of the inverter stage, which can not only realize reactive power compensation and voltage drop compensation but also realize the access of renewable energy and energy storage equipment and other functions[7-8].

Literature [9] proposed a structure of three-phase switching multi-winding PET applied to wind power generation systems. The system uses high-frequency AC links to achieve power conversion, which can not only improve power density and eliminate energy storage capacitors but also eliminate the common mode voltage of switching devices to reduce bearing current and increase system reliability. However, the influence of leakage inductance and stray inductance is not considered, and the ability to suppress fluctuations is poor, making it difficult to achieve soft switching. Literature [10] proposes a grid-connected permanent magnet synchronous wind turbine system based on a power electronic transformer. A supercapacitor energy storage device is added to the DC side so that the wind turbine has a strong low-voltage crossing ability. However, the increase in energy storage devices leads to an increase in system volume and cost and the complexity of the control strategy. Literature [11] also proposed a PMSG wind power generation system structure based on PET interface, studied the mathematical model and control strategy of each part of the system, analyzed the dynamic response of the system under different operating scenarios through modeling simulation and prototype experiments, and proved the power regulation characteristics of the PMG-SST system. However, the operation of the system under the fault state is not analyzed in detail. Literature [12] proposes the structure of a PET access PMSG wind power generation system with a single active bridge in the isolation stage, simplifying the system structure and control strategy. Simulation results show that the system can well cope with load changes and intermittent wind speed. Literature [13] proposes a voltage and power balance control strategy to control cascade multilevel PET based on single-phase vector control. In literature [14], SVPWM control technology was introduced to improve the operation performance of power electronic transformers. Literature [15] uses the fault isolation function of PET to alleviate the influence of voltage drop at common coupling points on wind turbine terminal voltage.

Therefore, this paper takes wind power generation as the research object, proposes a cascading connection mode of energy storage equipment and power electronic transformer, and proposes control strategies for power suppression, circulation suppression, capacitor voltage equalization, etc., by analyzing the PET topology and its control principle, to realize the smooth operation of wind power generation system.

2. Direct drive wind power system

2.1. Mathematical modeling of wind turbine

The basic principle of wind turbines is to use wind turbines to capture wind energy, convert it into mechanical energy, and transport it through the wind wheel shaft. From the knowledge of aerodynamics, the airflow power can be calculated as:

$$P_w = \frac{1}{2}\rho S V_W^3 \tag{1}$$

In equation (1): ρ is the atmospheric density, under the condition that the sea level temperature is $15^{\circ}C$, $\rho = 1.2kg/m^3$. S is the swept area of the impeller, (m^3). V_m is the wind speed.

The mechanical power output of the wind turbine is:

$$p_m = \frac{1}{2}\rho S V_W^3 C_P \tag{2}$$

In equation (1): C_p is the wind energy utilization coefficient.

By analyzing equation (2), it can be seen that the swept area S of the wind turbine is only related to the physical size of the impeller, and the atmospheric density ρ is generally regarded as a constant. Therefore, after the wind speed is given, the wind energy utilization coefficient C_p determines the power obtained by the wind turbine.

When the wind wheel rotates, the ratio of the blade tip speed to the input wind speed is defined as the blade tip speed ratio λ, whose expression is as follows:

$$\lambda = \frac{\omega_m R}{V_m} \tag{3}$$

In equation (3), ω_m is the impeller speed and R is the impeller radius.

Wind energy utilization coefficient C_p is a function of two variables: pulp distance Angle β and blade tip velocity ratio R, and its expression is as follows:

$$\begin{aligned} C_p(\lambda,\beta) &= 0.5176\left(\frac{116}{\lambda_i} - 0.4\beta - 5\right)^{-\frac{21}{\lambda_i}} + 0.0068\lambda \\ \frac{1}{\lambda_i} &= \frac{1}{\lambda + 0.08\beta} - \frac{0.035}{\beta^3 + 1} \end{aligned} \tag{4}$$

When the pulp distance Angle β takes different values, the relationship between wind energy utilization coefficient C_p and blade tip velocity ratio λ is shown in the figure. When the slurry distance Angle β increases, the wind energy utilization coefficient C_p decreases. For a fixed β, there is a unique λ to C_p reach the maximum, in which case λ is defined as the best tip ratio λ_{best}. When the blade's physical size is determined, there is a unique fixed value for the optimal tip ratio λ_{best}. As can be seen from Figure 1, when the pulp distance Angle β takes different values, the corresponding value $C_{p\max}$ is also different, according to the Betz limit, when $\beta = 0$, $C_{p\max} = 0.59$. However, under the current technical conditions, the wind energy utilization factor C_p of modern wind turbines is usually between 0.2 and 0.5.

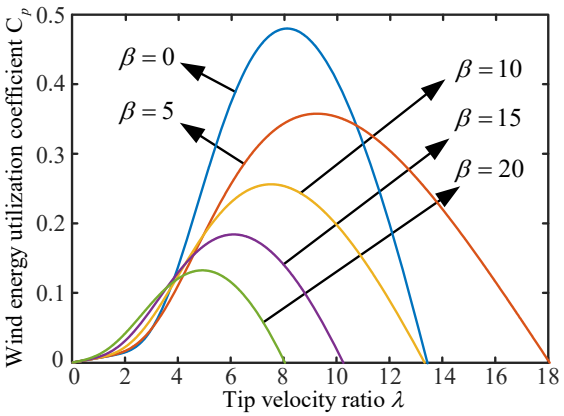

Figure 1. Relationship curve between blade tip velocity ratio and wind energy utilization coefficient

2.2. Converter control strategy for wind power generation system

2.2.1. Control strategy of wind turbine

In the converter control, the maximum wind energy of the wind turbine can be captured and the DC bus voltage can be maintained by controlling the generator speed. The vector control strategy of zero D-axis current is adopted in this scheme.

The voltage equation of the permanent magnet synchronous generator in the d-q coordinate system is as follows:

$$\begin{cases} u_{sd} = -R_s i_{sd} + \omega L_{sd} i_{sq} \\ u_{sq} = -R_s i_{sq} - \omega L_{sq} i_{sd} + \omega \psi_f \end{cases} \tag{5}$$

In equation (5), u_{sd}、u_{sq}、i_{sd} and i_{sq} are the components of stator voltage and current on the d-q axis coordinate system. L_{sd} and L_{sq} are the inductance of d and q axis of the stator winding. R_s is the armature resistance of the stator winding. ψ_f is the permanent magnet flux in the motor. ω is the angular velocity of the rotor.

When friction loss is ignored, the rotor motion equation is as follows:

$$\frac{d\omega}{dt} = \frac{n_p}{J}(T_e - T_L) \tag{6}$$

The electromagnetic torque equation is:

$$T_e = \frac{3}{2} n_p [\psi_f i_{sq} + (L_{sd} - L_q) i_{sd} i_{sq}] \tag{7}$$

When $i_{sd} = 0$ the electromagnetic torque equation can be simplified as:

$$T_e = \frac{3}{2} n_p \psi_f i_{sq} \tag{8}$$

It can be seen from equation (8) that the electromagnetic torque of the generator is directly proportional to the q-axis component of the stator current, and there is a linear relationship between the electromagnetic torque and the stator current. When the rotor flux ψ_f is constant, the electromagnetic torque T_e is only related to i_{sq}. The T_e^* is known, that the given reference value of the generator current can be obtained according to equation (8) :

$$\begin{cases} i_d^* = 0 \\ i_q^* = \dfrac{2T_e^*}{3n_p\psi_f} \end{cases} \tag{9}$$

It can be seen from equation (5) that there are coupling terms $\omega L_{sq} i_{sq}$ and $\omega L_{sd} i_{sd}$ between u_d and u_q, and a decoupling control needs to be introduced to eliminate the coupling between them. After taking $\omega L_{sq} i_{sq}$ and $\omega L_{sd} i_{sd}$ as feedforward compensation and introducing state feedback of i_{sd}, i_{sq} and ω, the voltage equation in d-q coordinate system is as follows:

$$\begin{cases} u_d^* = u_d - \omega L_{sq} i_{sq} \\ u_d^* = u_q + \omega L_{sd} i_{sd} \end{cases} \tag{10}$$

This decoupling control is called voltage feedforward decoupling control. The voltage feedforward decoupling control structure is shown in Figure 2.

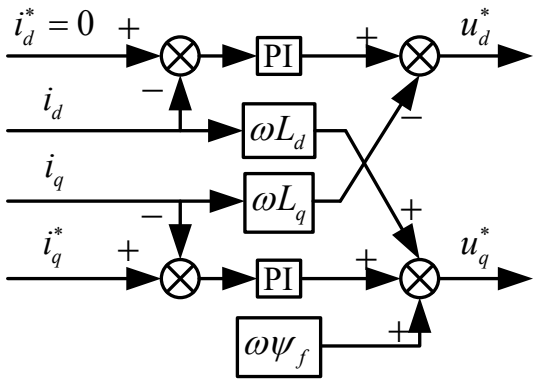

Figure 2. The voltage feedforward decoupling control structure

2.2.2. Grid side control strategy

Under the premise of direct current control, if the grid voltage vector is oriented, the active power and reactive power of the inverter can be controlled by controlling the amplitude and phase of the output of the grid-side converter, and the grid-connected control of the grid-side converter can be realized. This control method is called grid voltage-oriented vector control Strategy (VOC).

The synchronous rotating coordinate system is rotated according to the voltage V vector of the power grid, and the voltage vector remains recoupled with the d-axis. When $u_{gq} = 0$, according to the instantaneous power theory, the active power and reactive power of the system are:

$$\begin{cases} P_g = \dfrac{3}{2}(u_{gd} i_{gd} + u_{gq} i_{gq}) = \dfrac{3}{2} u_{gd} i_{gd} \\ Q_g = \dfrac{3}{2}(u_{gq} i_{gd} - u_{gd} i_{gq}) = -\dfrac{3}{2} u_{gd} i_{gq} \end{cases} \tag{11}$$

In equation (11), u_{gd}、u_{gq}、i_{gd} and i_{gq} are the voltage and current components of the grid voltage in the d and q axes.

Without considering the voltage fluctuation of the grid, $u_{gd} = 0$ is a constant value. According to equation (11), it can be seen that the instantaneous active power P_g and reactive power Q_g of the inverter are directly proportional to the current components i_{gd} and i_{gq} of the d and q axes. Therefore, the active power and reactive power of the grid-connected inverter can be controlled only by controlling the current component on the d-q axis.

The instantaneous active power input on the DC side is:

$$P = u_{dc} i_{dc} \tag{12}$$

Regardless of the loss of the inverter, the active power measured by AC is equal to the active power on the DC side, that is:

$$P_g = \frac{3}{2} u_{gd} i_{gd} = u_{dc} i_{dc} \tag{13}$$

According to equation (13), when the constant voltage of the grid is not considered and the loss of the inverter is ignored, the DC side voltage of the inverter can be controlled by controlling the active power i_{gd}.

The equation of the state of the inverter in the d-q coordinate system is:

$$\begin{cases} \dfrac{di_{gd}}{dt} = (u_{gd} - u_{di} + \omega_g L_g i_{gq}) / L_g \\ \dfrac{di_{gq}}{dt} = (u_{gq} - u_{qi} - \omega_g L_g i_{gd}) / L_g \end{cases} \tag{14}$$

In equation (14), ω_g is the angular frequency of the power grid. L_g is the inductance on the grid side, mainly to reduce the current distortion on the grid side. The grid side resistance is generally very small, the impact on the system is very small, can not be considered.

According to equation (14), the current of the d and q axes of the inverter is coupled with each other, and it is necessary to decouple them. When the current regulator uses PI to control the regulator, the output of the decoupling controller is:

$$\begin{cases} u_{di} = -\left(k_p + \dfrac{k_i}{s}\right)(i_{gd}^* - i_{gd}) + \omega_g L_g i_{gq} + u_{gd} \\ u_{qi} = -\left(k_p + \dfrac{k_i}{s}\right)(i_{gq}^* - i_{gq}) + \omega_g L_g i_{gd} + u_{gq} \end{cases} \tag{15}$$

In Equation (15), i_{gd}^* and i_{gq}^* are the reference values of the d-q axis current. By bringing equation (15) into equation (14), we get:

$$\begin{cases} \dfrac{di_{gd}}{dt} = \left(k_p + \dfrac{k_i}{s}\right)(i_{gd}^* - i_{gd}) / L_g \\ \dfrac{di_{gq}}{dt} = \left(k_p + \dfrac{k_i}{s}\right)(i_{gq}^* - i_{gq}) / L_g \end{cases} \quad (16)$$

Equation (16) shows that the differential equations of the current at the side of the d and q axes contain only the corresponding d and q axis components respectively, and the decoupling of the d and q axes is realized. The control structure diagram of the converter on the power grid side is shown in Figure 3.

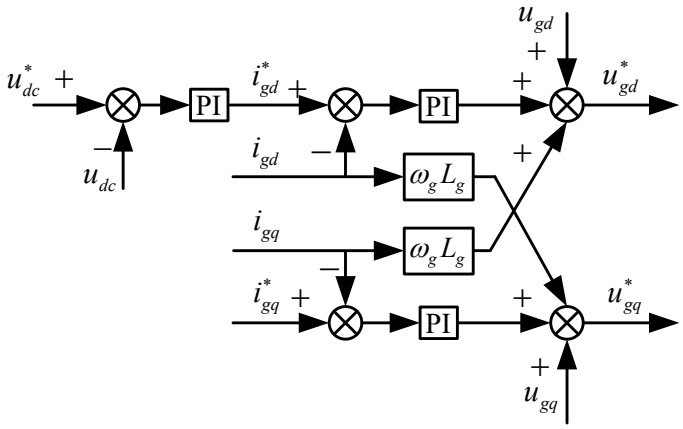

Figure 3. Grid side converter control structure diagram

3. Topology and Control Strategy of Power Electronic Transformers

With the development of society, the proportion of energy Internet in the new power system is increasing. A Power Electronic Transformer (PET) is the core equipment of the energy Internet. It can realize energy transmission and information transformation between ports, and organically integrate distributed microsources and multiple loads in the microgrid. It can operate independently and autonomously, and actively participate in the operation and management of the main power grid. Improve the information and intelligence level of the power grid. At present, PET is mainly composed of multiple MMC and DAB cascades.

3.1. MMC topology

The MMC consists of multiple sub-modules. Its topology structure is shown in Figure 4.

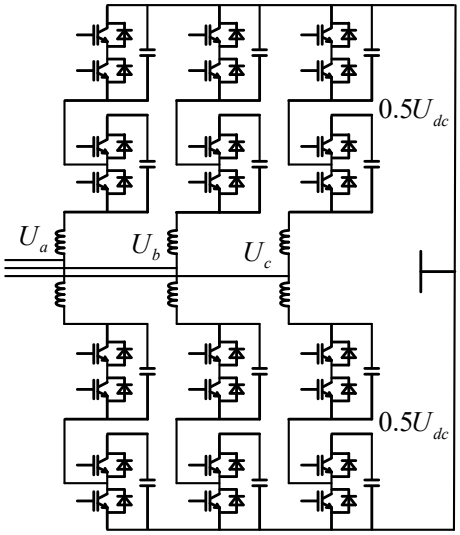

Figure 4. MMC topology structure

When used as an inverter, its left side is the direct current inlet of the grid, and the right side is the output of alternating current. When used as a rectifier, the connection port is reversed when used as an inverter. Through different control methods, the output AC can be controlled, and then the access voltage can be flexibly adjusted according to the different conditions of the power grid in the actual situation. Each bridge arm consists of several small modules (SM). The SM(half-bridge) topology structure diagram is shown in Figure 5. The working principle is: when there is a DC power supply flowing from the left positive direction, at the same time for the IGBT, the upper half is on and the lower half is off, so the current directly charges the capacitor through the above diode due to the characteristics of the IGBT/DIO, and the direction and size of the Uc are generally the same as the input voltage. This is engagement. The upper half of the IGBT turns off the lower half, so that when the current runs, it flows directly through the IGBT/DIO below, and the capacitor is neither charged nor discharged. This is the excision state. If the input direction of the current is opposite, the outflow is also opposite, the difference is that the capacitor is in the discharge state during the input stage.

In this way, by changing the on and off of the upper and lower IGBTs, the input and off state of SM can be changed. Then you can control the running state of the MMC.

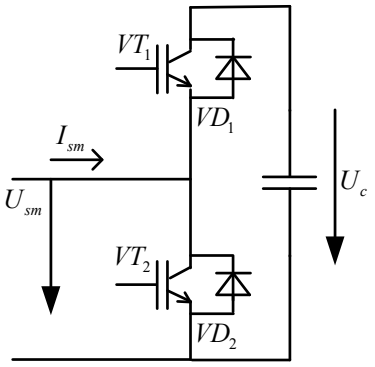

Figure 5. SM(half-bridge) topology structure diagram

3.2. Control policy of MMC

3.2.1. NLM modulation algorithm

Nearest Level Modulation (NLM) is the application of the integer function. To obtain the number of submodules in each phase of MMC in real-time, data should be rounded at the sampling point so that the output voltage on the AC side approximates the modulation wave. Its mathematical model is as follows:

$$n_p = \frac{N}{2} - \text{round}(\frac{V_s}{V_c}) \tag{17}$$

$$n_1 = \frac{N}{2} + \text{round}(\frac{V_s}{V_c}) \tag{18}$$

Where n_p and n_l are the number of submodules put into the upper and lower bridge arms respectively. VS is the instantaneous value of the modulating wave. VC is the average value of the capacitor voltage of the submodule.

The control period of MMC is related to the level number of NLM dynamic process. To ensure sufficient level number of output and avoid the quality of output voltage waveform being affected, the control frequency of MMC should meet the following requirements:

$$\pi f\sqrt{2NM} \le fc \le \pi fNM \tag{19}$$

Considering the time requirements of control operation, data acquisition, and communication in practical engineering, the control cycle of MMC is usually about 100us, and the corresponding control frequency is 10kHz.

3.2.2. Power and current double closed-loop control strategy

The mathematical model of A in MMC relative to MMC is analyzed, and its topological structure is shown in Figure 5.

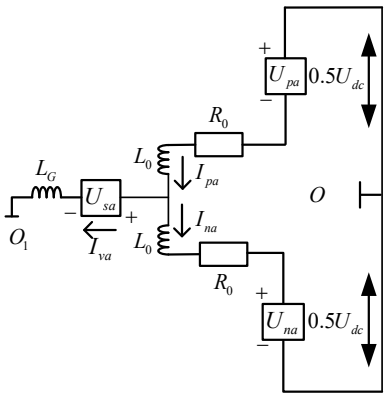

Figure 6. Topology diagram of phase A in MMC

According to Kirchhoff's law:

$$I_{va} = I_{pa} - I_{na} \tag{20}$$

$$U_{oo1} - U_{sa} = -\frac{U_{dc}}{2} + U_{pa} + R_0 I_{pa} + L_0 \frac{dI_{pa}}{dt} + L_G \frac{dI_{va}}{dt} \tag{21}$$

$$U_{oo1} - U_{sa} = \frac{U_{dc}}{2} - U_{na} - R_0 I_{na} - L_0 \frac{dI_{na}}{dt} + L_G \frac{dI_{va}}{dt} \tag{22}$$

Add equation (21) to equation (22) and substitute equation (20) into it to get:

$$2(U_{oo1} - U_{sa}) = (U_{pa} - U_{na}) + (L_0 + 2L_G)\frac{dI_{va}}{dt} + R_0 I_{va} \tag{23}$$

Assuming $U_{diff} = (U_{na} - U_{pa})/2$, equation (23) can be deformed to:

$$U_{oo1} - U_{sa} + U_{diff} = (\frac{L_0}{2} + L_G)\frac{dI_{va}}{dt} + \frac{R_0}{2} I_{va} \tag{24}$$

Equation (21) is subtracted from common (22) to obtain:

$$U_{dc} = U_{pa} + U_{na} + R_0(I_{pa} + I_{na}) + L_0(\frac{dI_{pa}}{dt} + \frac{dI_{na}}{dt}) \tag{25}$$

Assuming $U_{com} = (U_{na} + U_{pa})/2$ and $I_{cira} = (I_{na} + I_{pa})/2$, equation (25) can be transformed into:

$$\frac{U_{dc}}{2} = U_{com} + R_0 I_{cira} + L_0 \frac{dI_{cira}}{dt} \tag{26}$$

Assuming $R = \frac{R_0}{2}$ and $L = \frac{L_0}{2} + L_G$, the equation of equation (24) in the d-q axis coordinate system is:

$$\begin{cases} (LS + R)I_{vd} = -U_{sd} + U_{diffd} + \omega L I_{vq} \\ (LS + R)I_{vq} = -U_{sq} + U_{diffq} - \omega L I_{vd} \end{cases} \tag{27}$$

According to equation (27), the power and current controller structure of MMC is as follows:

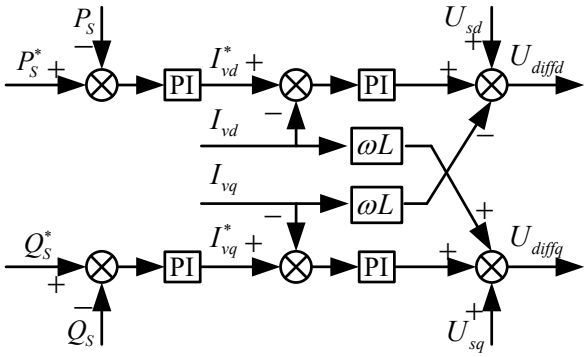

Figure 7. Power-current controller

3.2.3. Circulation suppression control strategy

The expression of three-phase upper arm current I_{lu} and three-phase lower arm current I_{lv} of MMC is as follows:

$$\begin{cases} I_{lu} = \frac{1}{3}I_{dc} + \frac{1}{2}I_1\cos(\omega_1 t + \varphi_{I1} + \beta_l) \\ I_{lv} = \frac{1}{3}I_{dc} - \frac{1}{2}I_1\cos(\omega_1 t + \varphi_{I1} + \beta_l) \end{cases} \tag{28}$$

In equation (28), I_1 and φ_{I1} are the amplitude and phase of the fundamental frequency component of AC. ω_1 is the fundamental angular frequency. β_l is the three-phase phase

shift angle.

Under the charge and discharge action of the bridge arm current on the capacitor, the expression of the three-phase upper bridge arm capacitor voltage U_{Clu} and the three-phase lower bridge arm capacitor voltage U_{Clv} is as follows:

$$\begin{cases} U_{Clu} = U_{dc} + \dfrac{1}{6C_{eq}}[I_{dc} - \dfrac{3}{4}M_1 I_1 \cos(\varphi_{u1} - \varphi_{I1})]t + \\ \quad \dfrac{I_1}{4\omega_1 C_{eq}}\sin(\omega_1 t + \varphi_{I1} + \beta_l) - \\ \quad \dfrac{M_1 I_{dc}}{6\omega_1 C_{eq}}\sin(\omega_1 t + \varphi_{u1} + \beta_l) - \\ \quad \dfrac{M_1 I_1}{16\omega_1 C_{eq}}\sin(2\omega_1 t + \varphi_{u1} + \varphi_{I1} + 2\beta_l) \\ U_{Clv} = U_{dc} + \dfrac{1}{6C_{eq}}[I_{dc} - \dfrac{3}{4}M_1 I_1 \cos(\varphi_{u1} - \varphi_{I1})]t - \\ \quad \dfrac{I_1}{4\omega_1 C_{eq}}\sin(\omega_1 t + \varphi_{I1} + \beta_l) + \\ \quad \dfrac{M_1 I_{dc}}{6\omega_1 C_{eq}}\sin(\omega_1 t + \varphi_{u1} + \beta_l) - \\ \quad \dfrac{M_1 I_1}{16\omega_1 C_{eq}}\sin(2\omega_1 t + \varphi_{u1} + \varphi_{I1} + 2\beta_l) \end{cases} \tag{29}$$

In equation (29): $M_1 = \dfrac{2U_1}{U_{dc}}$ is the fundamental modulation ratio. U_1 and φ_{u1} are the amplitude of the fundamental frequency component of the AC voltage. C_{eq} are the equivalent capacitance of the bridge arm.

According to equation (29), the capacitor voltage of the bridge arm contains not only the DC component but also the fundamental frequency and double-frequency AC component. The double-frequency AC component is the main component of the bridge arm circulation, which will distort the current of the bridge arm, so it is very important to suppress it.

The design idea of the loop suppression controller is the same as that of the power current controller. Equation (29) is decomposed into the voltage equation in the d-q axis coordinate, and the double frequency AC component is decoupled. The structure of the circulation controller is shown in Figure 8.

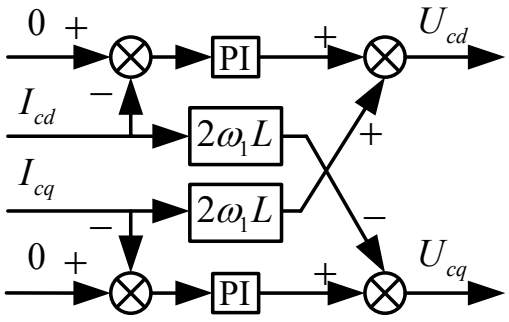

Figure 8. Circulation suppression controller

3.3. DAB topology and control strategy

Dual active bridge DC converter (DAB) is often used in the isolation stage of three-stage PET because of its advantages of electrical isolation and bidirectional power transmission. The basic topology diagram is shown in Figure 9.

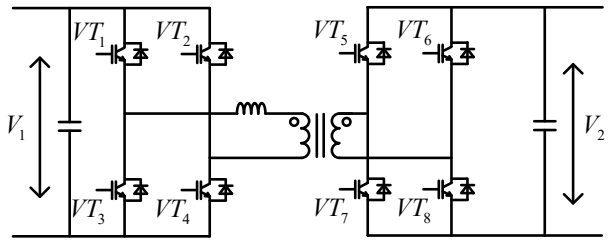

Figure 9. DAB topology structure diagram

Most DAB control methods are phase-shifted carrier control. The sps modulation method is used this time. Specifically, the energy flow of the double-active bridge is regulated by changing the phase angle of the AC source at both ends. In a double-active bridge, the input DC voltage is converted into a high-frequency square wave by a first-side full-bridge converter. After voltage conversion by a high-frequency transformer, the output DC voltage is rectified by a second-side full-bridge converter. The energy transmission can be controlled by adjusting the phase shift of the full bridge at both ends in the double-active bridge, so as to complete the voltage conversion.

4. Simulation Analysis

The structure diagram of the air storage system based on PET is shown in Figure 10. The simulation model was built in MATLAB/Simulink. The initial wind speed was 10m/s, which dropped to 4m/s after 1.2s. The DC bus voltage of the high voltage side of the DAB module is 3000V, and the DC bus voltage of the low voltage side is 700V. At 1s, the circulation suppression controller began to be added to the system to suppress the circulation.

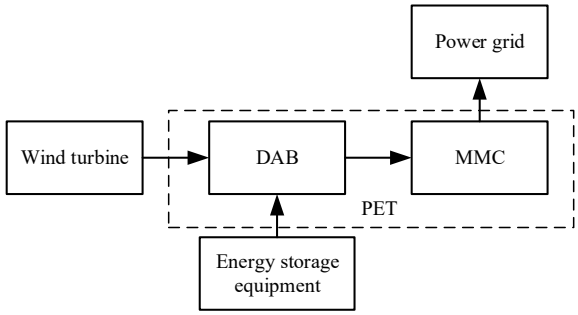

Figure 10. Structure diagram of air storage system based on PET

The voltage waveform of the bus on the DC side of the air storage system is shown in Figure 11. The wind power system combined with the hybrid energy storage system can stabilize the DC side of the wind storage module at about 3000V by improving the voltage control strategy. In 1.2 seconds, the wind speed of the wind power system decreases from 10 meters per second to 4 meters per second, making the system output power drop sharply. However, due to the power compensation and suppression of the energy storage equipment and DAB, the bus voltage of the DC side is maintained at 3000V.

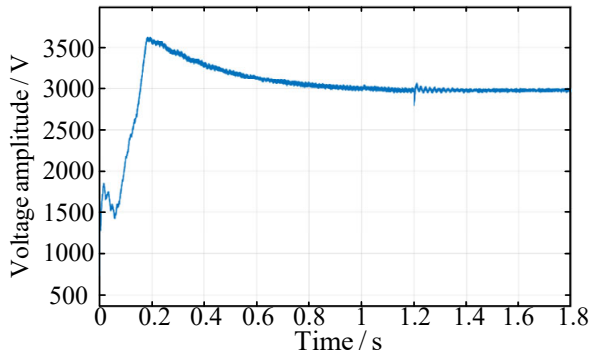

Figure 11. DC bus voltage waveform of wind storage power generation system

The energy storage device system is connected to the low-voltage DC side of DAB, and the voltage of the DC bus is stabilized at about 700V through the voltage outer loop control of the energy storage device. DAB low-voltage DC bus voltage output waveform is shown in Figure 12. DAB HVDC bus voltage output waveform is shown in Figure 13.

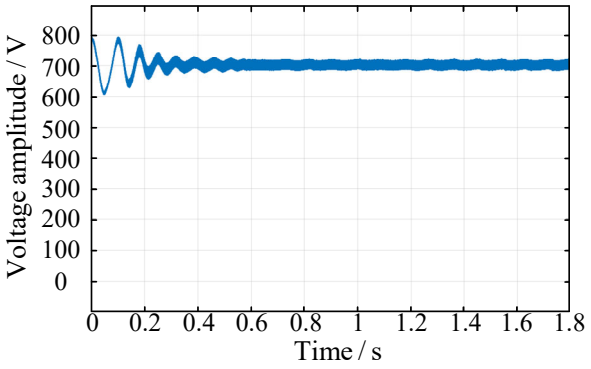

Figure 12. DAB low voltage DC bus voltage output waveform

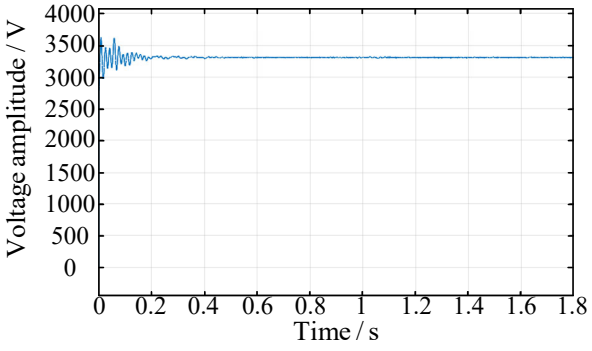

Figure 13. DAB HVDC bus voltage output waveform

As can be seen from Fig. 14 MMC grid-connected port output voltage and Fig. 15 Comparison of internal circulation control before and after MMC, the DC bus can reach the required 3000v, and DAB can make the current of the high voltage side and the low voltage side reach the corresponding value. When the MMC is connected to the grid, the power control can be realized, and the harmonic reduction of the internal circulation of the MMC can be seen obviously after the circulation suppressor is added.

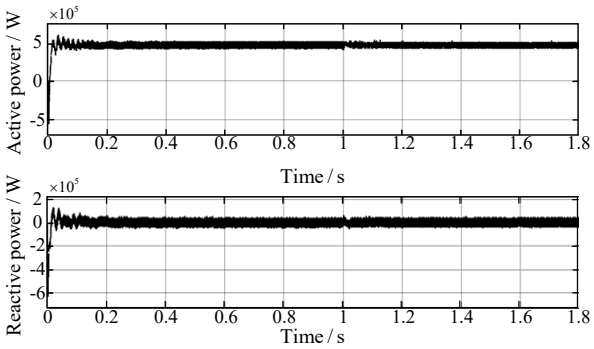

Figure 14. MMC grid-connected port output voltage

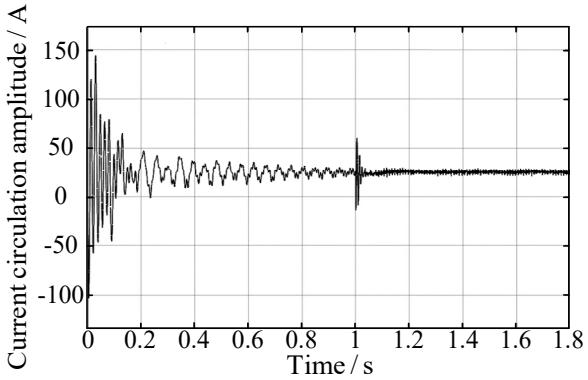

Figure 15. Comparison of internal circulation control before and after MMC

5. Conclusion

Based on the working principle, topology structure, and grid-connected requirements of PET, a PET topology applied to the grid-connected system of wind power is proposed in this paper. The DAB low-voltage DC bus terminal is connected to the energy storage device. A coordinated control strategy for the grid-connected wind storage system is presented, and the effectiveness of the proposed control strategy for calming wind power fluctuations is verified by simulation analysis.

Acknowledgment

This work was supported in part by a grant from the Innovation Fund of Postgraduate, Sichuan University of Science and Engineering (Y2022140).

References

[1] XIAO Ya-ping, XIAO sa, REN Bei-ting, et al.Study on the Operation of VSCF Doubly Fed Wind Power Generator[J]. JOURNAL OF ELECTRIC POWER ,2017,32(05):370-375.

[2] LI Huabo, XIE Yongchao, HU Yang . Research on Variable Pitch Linear Active Disturbance Rejection Control Sys-tem for Doubly Fed Wind Power Generation System. HENAN SCIENCE,2021,39(02):190-195.

[3] Shi J, Lee W J, Liu X. Generation scheduling optimization of wind-energy storage system based on wind power output fluctuation features[J]. IEEE Transactions on Industry Applications, 2017, 54(1): 10-17.

[4] Wu X, Jiang Y. Source-network-storage joint planning considering energy storage systems and wind power integration[J]. IEEE Access, 2019, 7: 137330-137343.

[5] Zhai Y, Zhang J, Tan Z, et al. Research on the application of superconducting magnetic energy storage in the wind power generation system for smoothing wind power fluctuations[J]. IEEE Transactions on Applied Superconductivity, 2021, 31(5): 1-5.

[6] CHEN Hong. Discussion on Energy Storage Technologies in Wind Power Integration [J]. Electrical technology, 2019 (18): 133-134.

[7] Zhao T, Wang G, Bhattacharya S, et al. Voltage andpower balance control for a cascaded h ― bridge converter-based solid-state transformer [J]. IEEE Transactions on Power Electronics, 2013, 28(4):1523-1532.

[8] Wang Ting, Wang Guangzhu, Zhang Xun. The control strategy of power elec-tronic transformer based on modular multilevel matrix con-verters [J]. Transactions of ChinaElectrotechnical Society, 2016, 31(18):108-115.

[9] Vipin V N, Venkatramanan D, Mohan N. An Online-Optimization-Based High-Frequency Link Control of an MMC-Driven Power Electronic Transformer for Wind-Energy Systems[J]. IEEE Transactions on Energy Conversion, 2023.

[10] Zhang Mingrui, ChenJie, Wang Zhixin, et al. A new permanent magnet synchronouswind-power generation grid-connected system)［J］. Power System Protection and Con-trol, 2013, 41(14):141-148.

[11] Gao R, She X, Husain I, et al. Solid-state-transformer-interfaced permanent magnet wind turbine distributed generation system with power management functions[J]. IEEE Transactions on Industry Applications, 2017, 53(4): 3849-3861.

[12] Tom B M, Ashok S. Solid state transformer for wind powerinterfacing [A]. 2017 IEEE International Conference onSignal Processing, Informatics, Communication and Energy Systems(SPICES) [C]. 2017.1-6.

[13] Zhu L, Zhang F, Jin S, et al. Optimized power error comparison strategy for direct power control of the open-winding brushless doubly fed wind power generator[J]. IEEE Transactions on Sustainable Energy, 2018, 10(4): 2005-2014.

[14] Zhang Mingrui, Liu Jinhui, Jin Xin. Research on the SVPWM solid state transformer appliedin smart micro-grid [J]. Transactionsof China Electrotechnical Society, 2012, 27(1): 90-97.

[15] Syed I, Khadkikar V. Replacing the grid interface trans-former in wind energy conversion system with solid ― statetransformer [J]. IEEE Transactions on Power Systems, 2017, 32(3):2152-2160.